Low-NEP Room-Temperature Broadband THz Direct Detection with a 0.13-µm SiGe HBT Device

J. Grzyb, M. Andree, R. Jain, B. Heinemann[1], U. R. Pfeiffer
IHCT, Bergische Universität, Rainer-Gruenter-Str. 21, D-42119 Wuppertal, Germany
[1] IHP- Leibniz-Institut für Innovative Mikroelektronik, D-15236, Frankfurt Oder, Germany

***Abstract*— This paper reports on the influence of internal device parasitics of a high-speed SiGe HBT, its bias operation range, and circuit-antenna co-design aspects on frequency-dependent rectification efficiency of the room-temperature operated antenna-coupled THz direct detectors in 130-nm technology leading to their low-NEP operation in a near-THz fractional bandwidth. In particular, an optical NEP below 36 pW/√*Hz* was measured across 220-1000 GHz for the single and dual linearly-polarized detectors with minimum NEP values of 1.9 pW/√Hz at 292 GHz and 2.7 pW/√Hz at 449 GHz for the former and the latter, respectively.**

I. INTRODUCTION

DUE to low sensitivity of the room-temperature operated THz direct detectors, they require a large fractional RF bandwidth toward future passive imaging. For silicon technologies, the most common class of direct detectors relies on the concept of non-quasistatic self-mixing in the MOSFET channel [1,2,3] and considerably less work is devoted to THz rectification by the base-emitter junction nonlinearity of a SiGe HBT [4,5,6]. However, the most recent advancements in SiGe HBT technologies have reported the fastest devices with ft/fmax of 500/700 GHz [7] and although both figures of merit are achieved at sufficiently high bias current densities and refer to the collector node, the THz rectification efficiency in terms of detector responsivity profits from scaling of internal device parasitics around the base and emitter nodes.

In this contribution, various device operation and implementation aspects altogether with antenna-circuit co-design challenges [8] are addressed to maximize the detector operation bandwidth in terms of responsivity and NEP. In particular, we demonstrate for the first time that the HBT device can be operated as a THz direct detector not only in the forward active region but also in saturation with zero-bias current; the bias range largely ignored due to the generally limited dc and ac performance.

II. DETECTOR DETAILS

Fig.1 presents the chip micrograph of a 3×3 array of detectors and the simplified circuit schematics of the selected single and dual linearly-polarized pixels implemented with the minimum-size devices (1×0.12µm^2) in an advanced 0.13-µm SiGe HBT technology with ft/fmax of 350/550 GHz. The dual-polarization version comprises two separate detection channels supporting two orthogonally-oriented linear polarizations to operate with unpolarized light; a useful feature for imaging application. Each detection path consists of a transistor pair in common-base (CB) configuration placed in the pixel center and is driven differentially from the corresponding silicon lens-coupled wire ring antenna, through the chip bottom side. The rectified DC signal, either current or voltage, is collected at the output collector node. With perfect layout symmetry, a virtual ac ground is established at the base and collector external nodes for differential RF signals, providing inherent isolation between input THz and output dc paths.

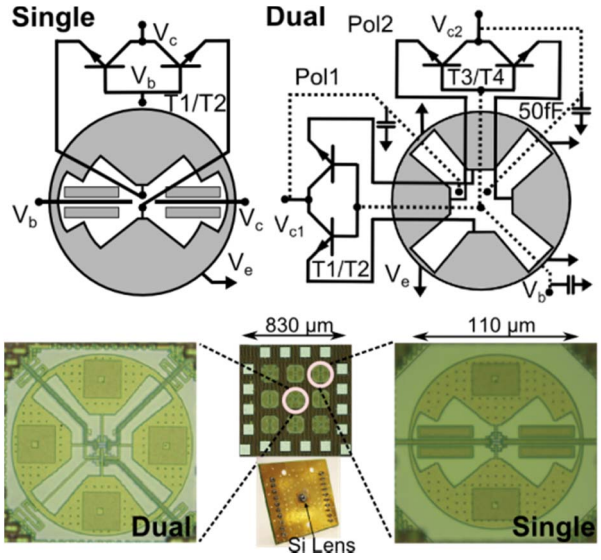

Fig.1 Chip micrograph of an array of SiGe HBT detectors with the simplified circuit schematics of the single and dual linearly-polarized detector versions.

All detectors were operated in voltage mode with a voltage drop induced by the rectified THz collector current across the detector output resistance taken as an output signal. Two distinctive bias regions were investigated: forward-active and saturation. In the former, the detector output resistance is equivalent to the externally applied load resistance (1.83 kΩ for our setup) and the voltage responsivity is simply a linear function of the rectified current. For the saturation, however, the detector output resistance is a nonlinear function of the transistor bias voltages, similarly to the current responsivity, and, therefore, the optimum bias operation in this case differs from that in the forward-active region. In particular, the external resistor can be completely removed and the collector node left unbiased, resulting in zero-power consumption comparable to a cold MOSFET channel operation. Although, the dynamic (ac) low-frequency current gain for the device in saturation is lower than for forward-active region, the collector shot noise becomes negligible at the same time, and the detector output noise floor is dominated by thermal noise. To minimize the influence of the base shot-noise on the detector NEP, the base nodes were biased from low-impedance and low-noise power supply units, independently from the detector operation range. For the device in forward-active region, the base-emitter voltage minimizing NEP is around 760-780mV and corresponds to the point where two effects influencing the rectified current are optimally traded. The first is related to the

optimum nonlinearity for the base-emitter junction and the other is about the maximum internal base-emitter driving voltage. The internal base-emitter driving voltage, in turn, shows a strong frequency-dependence resulting from the internal device parasitics and the antenna input impedance. For the detector operating in saturation, the optimum bias voltage moves to around 670mV due to additional influence of the device output resistance which drops with increasing V_{be}.

The key internal device parasitics influencing THz (above 300 GHz) rectification are the base and emitter contact resistances altogether with the nonlinear base-emitter capacitance. The influence of emitter resistance, creating a series feedback path, is of particular importance independently from the operation frequency. This resistance is responsible for linearization of the internal base-emitter diode and prevents the internal base-emitter voltage from effective growth for higher bias current densities. In combination with C_{be}, it creates a low-pass transfer function that deteriorates the detector responsivity above 500 GHz. Another major time constant is created by the presence of a base resistance with even stronger influence on the detector responsivity toward 1THz. Finally, the detector maximum available responsivity with the corresponding antenna input impedance maximizing this responsivity are both strong functions of frequency with a generally low-pass behavior defined by multiple time constants.

As the antenna-coupled detectors are intended for broadband operation with a near 1 THz operational BW, an extensive search space of the driving antenna impedances, maximizing the detector responsivity across the operational BW and the transistor bias point, has been performed with the aid of Harmonic Balance simulations and the HiCUM device model. It should be noted that efficient exploitation of this bandwidth with a classical design relying on the cascaded circuit and the antenna placed side by side is very unlikely and calls for direct antenna-circuit co-design. Furthermore, synthesizing an antenna geometry that ideally mimics the optimum frequency-dependent input impedance becomes a challenging task. Therefore, the sensitivity of the detector responsivity to the antenna impedance deviating from optimum was studied, and the antenna geometry was optimized in view of the global detector responsivity across 1THz band [8].

III. Results

The detector array was assembled with a 3-mm diameter hyper-hemispherical silicon lens without AR coating and characterized in the antenna far-field range with a set of antenna-equipped electronically-chopped precalibrated power extension modules from OML, VDI, and AB Millimetre. The detector responsivity was determined from the Friis transmission formula and the measured directivity of the lens-coupled on-chip antenna. Therefore, it is normalized to the antenna effective aperture of an isotropic radiator (0 dBi directivity), but includes all optical losses in the receive path such as Fresnel loss at the lens aperture, antenna radiation efficiency, and antenna-detector mismatch. The NEP was calculated from the ratio of detector output noise spectral density at the chopping frequency (100 kHz) and the corresponding responsivity. The measured optical NEP across 220-1000 GHz for both detector versions operating in the forward-active region is presented in Fig. 2. The NEP stays below 36 pW/√Hz in the entire measured frequency range with the minimum values of 1.9 pW/√Hz at 292 GHz and 2.7 pW/√Hz at 449 GHz for the single and dual-polarized detector, respectively. For the device operating in saturation with V_{CE} = 0V, the minimum NEP values increase to 5.1pW/√Hz and 8.2pW/√Hz, correspondingly. The growing NEP values for lower frequencies correspond to the lower end of the antenna operation bandwidth whereas an increase of NEP above 500 GHz is predominantly related to the aggregate influence of the previously discussed internal device parasitics. The NEP differences between single- and dual-polarized detectors are related to different antenna implementation losses in both cases [8].

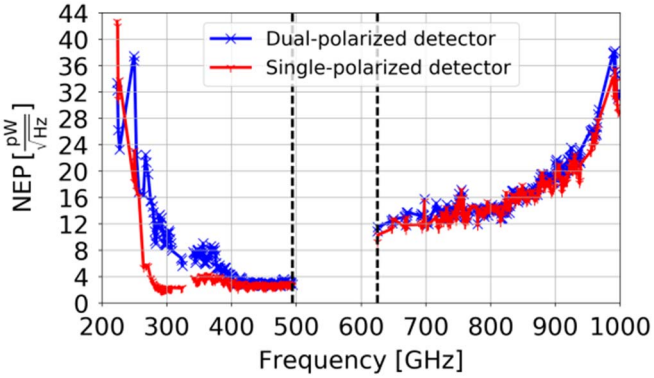

Fig.2. Measured optical NEP for single and dual-polarized detectors. The transistors are biased in the forward-active region. The 500-620 GHz band is not covered due to the lack of equipment. The measurements were performed in voltage mode with 1.8 kΩ load resistors at the output collector nodes.

REFERENCES

[1] R. Jain, R. Zatta, J. Grzyb et al., "A Terahertz Direct Detector in 22nm FD-SOI CMOS," in 13th European Microwave Integrated CircuitsConference (EuMIC), Sept 2018, pp. 25–28.

[2] J. Grzyb et al., "Real-time video rate imaging with a 1 k-pixel THz CMOS focal plane array," Proc. SPIE, vol. 8362, pp. 1–12, May 2012.

[3] S. Boppel et al., "CMOS integrated antenna-coupled field-effect transistors for the detection of radiation from 0.2 to 4.3 THz," IEEE Trans. Microw. Theory Techn., vol. 60, no. 12, pp. 3834–3843, Dec. 2012.

[4] M. Andree, J. Grzyb, R. Jain et al., "A Broadband Dual-Polarized Terahertz Direct Detector in a 0.13-µm SiGe HBT Technology," in IEEE Int. Microwave Symposium Conf. (IMS), 2019, pp. 500–503.

[5] M. Andree, J. Grzyb, R. Jain et al., "A Broadband Antenna-Coupled Terahertz Direct Detector in a 0.13-µm SiGe HBT Technology," in European Microwave Int. Circ. Conf. (EuMIC), 2019, pp. 168–171.

[6] Z. Li, B. Qi, X. Zhang, S. Zeinolabedinzadeh, L. Sang, and J. Cressler, "A 0.32 THz SiGe imaging array with polarization diversity," IEEE Trans. THz Sci. Technol., vol. 8, no. 2, pp. 215–223, Mar. 2018.

[7] B. Heinemann et al., "SiGe HBT with ft/fmax of 505 GHz/720 GHz," in Proc. IEEE Int. Electron Devices Meeting, Dec. 2016, pp. 3.1.1–3.1.4.

[8] J. Grzyb, M. Andree, R. Jain et al., "A Lens-Coupled On-Chip Antenna for Dual-Polarization SiGe HBT THz Direct Detector," IEEE Ant. Wireless Propag. Lett.,vol. 18, no.11, pp. 500–503, Nov. 2019.